

Multi-Scale Finetuning for Encoder-based Time Series Foundation Models

Zhongzheng Qiao^{1,2,3} Chenghao Liu⁴ Yiming Zhang¹ Ming Jin⁵ Quang Pham⁴

Qingsong Wen⁶ P.N.Suganthan⁷ Xudong Jiang¹ Savitha Ramasamy^{2,3}

Abstract

Time series foundation models (TSFMs) demonstrate impressive zero-shot performance for time series forecasting. However, an important yet underexplored challenge is how to effectively finetune TSFMs on specific downstream tasks. While naive finetuning can yield performance gains, we argue that it falls short of fully leveraging TSFMs’ capabilities, often resulting in overfitting and suboptimal performance. Given the diverse temporal patterns across sampling scales and the inherent multi-scale forecasting capabilities of TSFMs, we adopt a causal perspective to analyze finetuning process, through which we highlight the critical importance of explicitly modeling multiple scales and reveal the shortcomings of naive approaches. Focusing on *encoder-based* TSFMs, we propose **MultiScale FineTuning (MSFT)**, a simple yet general framework that explicitly integrates multi-scale modeling into the finetuning process. Experimental results on three different backbones (MOIRAI, MOMENT and UNITS) demonstrate that TSFMs finetuned with MSFT not only outperform naive and typical parameter efficient finetuning methods but also surpass state-of-the-art deep learning methods.

1 Introduction

Time series foundation models (TSFMs) have emerged as a transformative direction within the time series forecasting (TSF) community [2, 42, 8]. By pretraining on extensive time series datasets, these models possess universal knowledge, enabling them to achieve impressive zero-shot performance on various forecasting tasks. Despite significant advancements in TSFM research, current studies predominantly focus on model pretraining and zero-shot evaluation, while paying limited attention to the critical challenge of effectively finetuning these universal models for specific downstream tasks. In contrast, finetuning pretrained models has become the standard pipeline for real-world applications in domains such as natural language processing (NLP) and computer vision (CV). Research in these fields has revealed key challenges in finetuning foundation models, including preserving pretrained knowledge [24], avoiding overfitting [15], and ensuring efficient adaptation [13, 47].

Existing finetuning strategies for TSFMs often rely on naive approaches, such as full finetuning or linear probing [2, 12, 11]. While these methods may offer performance gains, we argue that **naive finetuning is suboptimal for TSFMs** as it fails to account for the intrinsic *multi-scale properties* of both time series data and TSFMs. As a data modality generated from continuous real-world processes, time series are inherently entangled and can be decomposed across multiple scales [23, 18]. A time series can exhibit distinct temporal patterns at different sampling scales. For instance, as shown in

¹Nanyang Technological University. ²Institute for Infocomm Research, A*STAR. ³CNRS@CREATE. ⁴Salesforce AI Research. ⁵Griffith University. ⁶Squirrel Ai Learning. ⁷Qatar University. Mail to: Zhongzheng Qiao <qiao0020@e.ntu.edu.sg>, Chenghao Liu <chenghao.liu@salesforce.com>.

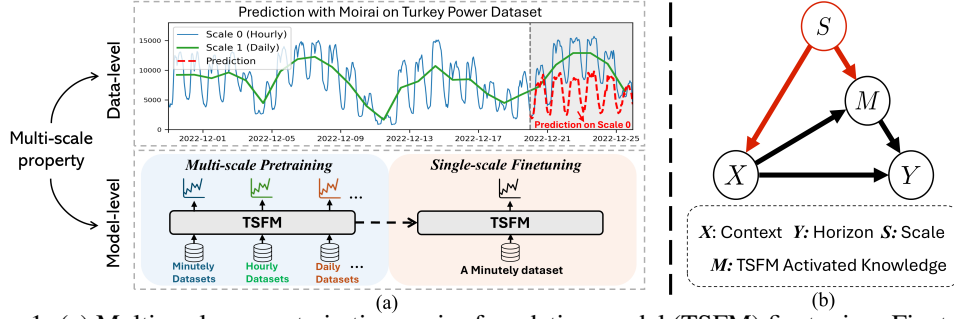


Figure 1: (a) Multi-scale property in time series foundation model (TSFM) finetuning. Finetuning TSFMs on the original scale may overlook potential temporal patterns in time series and underutilize their multi-scale forecasting capabilities learned during pretraining. (b) Causal graph for forecasting of TSFMs. Nodes denote the abstract data variables and directed edges denote the causality, i.e. cause \rightarrow effect. Scale S acts as a confounder, influencing both input context series X and model’s activated knowledge M (shown in red).

Figure 1 (a), energy consumption measured at the hour level shows micro-scopic local usage patterns, whereas daily records suppress these finer details, highlighting macro-scopic consumption trends instead. This multi-scale nature poses additional challenges, as naive finetuning tends to overfit the model to patterns at the original scale, overlooking the latent dynamics that prevail at coarser scales. From a modeling perspective, TSFMs pretrained on extensive, multi-scale datasets are inherently equipped with robust multi-scale forecasting capabilities. However, naive finetuning fails to harness this potential, as it restricts learning to the original scale. Consequently, it underutilizes the pretrained knowledge of TSFMs, capturing only partial temporal patterns. Such failure not only limits the generalizability of TSFMs across scales but also leads to suboptimal downstream performance.

To address the aforementioned challenge, we begin by analyzing the finetuning process of TSFMs through a causal lens. The relationship among key variables is shown in Figure 1(b). Specifically, the objective of finetuning is to adapt the model $P(Y|X)$ to capture temporal patterns and better predict the horizon Y given the context X . However, the presence of scale S as a confounder introduces spurious correlations between context X and the knowledge M activated within TSFM, causing the model to rely on correlations that lack causal grounding. Directly forecast with $P(Y|X)$ would mistakenly associate non-causal but positively correlated context X to horizon Y . To overcome this, we propose using the interventional distribution $P(Y|do(X))$, which isolates the true causal effect of X on Y by blocking the influence of the confounder S . We will elaborate on how this is achieved through backdoor adjustment [27] in Section 3.

This causal perspective highlights the need for explicitly modeling multiple scales during TSFM finetuning. However, integrating multi-scale modeling in this context remains underexplored and presents several non-trivial challenges—despite its success in standard time series forecasting modeling [34, 41, 40]. **First**, most TSFMs tokenize time series through patching [25], resulting in tokens at different scales exhibiting varying resolutions and temporal dynamics. This discrepancy complicates the finetuning of the unified input projection and attention weights. **Second**, applying attention across multi-scale tokens can introduce spurious dependencies due to misaligned time indices, making it difficult to capture true temporal relationships. Thus, the attention mechanism must account for or bypass index-related biases. **Finally**, since the model produces separate predictions at each scale, effectively aggregating these multi-scale outputs is essential for accurate and robust forecasting.

To close the gap, we propose a novel encoder-based TSFM finetuning framework using multi-scale modeling, namely **MSFT**. Our contributions are summarized as follows:

1. Building on causal insights, we identify the limitations of naive finetuning for TSFMs and propose a multi-scale modeling approach for TSFM finetuning. To the best of our knowledge, this is the first work to introduce multi-scale modeling into TSFMs.
2. We propose MSFT, a simple yet effective finetuning framework for encoder-based TSFMs. MSFT begins by downsampling time series into multiple scales and independently tokenizing each scale at its own resolution. Scale-specific modules are applied to the input projection and attention layers to activate scale-specific knowledge. Decoupled dependency modeling is then performed on the concatenated multi-scale sequence, enabling the model to capture both within-scale (via

in-scale attention) and cross-scale (via cross-scale aggregator) dependencies. Finally, a learnable weighting strategy is employed to aggregate the multi-scale prediction results.

3. Our extensive evaluation on various datasets for Long Sequence Forecasting [43] and Probabilistic Forecasting [42] demonstrates that **MSFT** not only significantly improves the finetuning results of TSFMs but also surpasses other state-of-the-art models trained from scratch.

2 Preliminaries

Problem Formulation. We first define the TSF task, in which the model predicts a horizon window given a context window. Let C denote the context length and H the horizon length. Context window $\mathbf{X} \in \mathbb{R}^{C \times D}$ and horizon window $\mathbf{Y} \in \mathbb{R}^{H \times D}$ are consecutively extracted from the same time series $\mathbf{x}_{1:T} = (\mathbf{x}_1, \mathbf{x}_2, \dots, \mathbf{x}_T)$, where D is the feature dimension at each time step. The sample at time step t is denoted as $(\mathbf{X}_t, \mathbf{Y}_t)$, where $\mathbf{X}_t = (\mathbf{x}_{t-C}, \dots, \mathbf{x}_{t-1})$ and $\mathbf{Y}_t = (\mathbf{x}_t, \dots, \mathbf{x}_{t+H-1})$. Given a model parameterized by θ and a training dataset $\mathcal{D}^{\text{train}} = \{(\mathbf{X}_t, \mathbf{Y}_t)\}_{t=1}^{T_o}$, the objective is to learn the model parameter θ^* to achieve minimum error on the testing set $\mathcal{D}^{\text{test}} = \{(\mathbf{X}_t, \mathbf{Y}_t)\}_{t=T_o+1}^T$.

Multi-Scale Generation. In multi-scale modeling, the standard approach for generating multi-scale sequences is based on *average pooling* [34, 41]. Given a training sample (\mathbf{X}, \mathbf{Y}) , both context and horizon windows are downsampled into multiple temporal scales using non-overlapping average pooling. Specifically, downsampling factor is commonly set to 2, resulting in a set of scales defined by $1, 2, \dots, 2^K$, where K is the number of downsampled scales. Let \mathcal{S} denote the set of multi-scale time series as $\mathcal{S} = \{\mathbf{S}_0, \dots, \mathbf{S}_K\}$, where $\mathbf{S}_i = (\mathbf{X}^i, \mathbf{Y}^i)$ corresponds to the i -th scale series, formed by concatenating the downsampled context $\mathbf{X}^i \in \mathbb{R}^{C_i \times D}$ and downsampled horizon $\mathbf{Y}^i \in \mathbb{R}^{H_i \times D}$. Here, $C_i = \lceil \frac{C}{2^i} \rceil$ and $H_i = \lceil \frac{H}{2^i} \rceil$. Note that \mathbf{S}_0 represents the input series at the original scale.

Encoder-based TSFM. We outline the architectural framework of existing encoder-based TSFMs [42, 12, 11] from a high-level perspective. These models adopt an encoder-only Transformer [38] architecture and segment univariate time series into a sequence of patch tokens [25]. While multivariate extensions are supported in some models [42, 11], we focus on the univariate case for illustration ($D = 1$), without loss of generality. The pretraining is conducted by masked reconstruction [9]. Given a time series (\mathbf{X}, \mathbf{Y}) , the series is segmented into non-overlapping patch tokens of size P , resulting in a sequence of patches $\mathbf{x} \in \mathbb{R}^{N \times P}$, where $N = \lceil \frac{C}{P} \rceil + \lceil \frac{H}{P} \rceil$. The goal is to forecast the predictive horizon by $\hat{\mathbf{Y}} = f_\theta(\mathbf{x})$, where f_θ is a transformer with the block number L and model dimension d . Specifically, Equation 1 represents the procedure of calculating $\hat{\mathbf{Y}} = f_\theta(\mathbf{x})$:

$$\mathbf{h}^0 = \text{InProject}(\mathbf{x}); \quad \mathbf{h}^l = \text{AttnBlock}(\mathbf{h}^{l-1}), l = 1, \dots, L; \quad \hat{\mathbf{Y}} = \text{OutProject}(\mathbf{h}^L) \quad (1)$$

Let $\mathbf{h}^l \in \mathbb{R}^{N \times d}$ represent the token embeddings produced by layer l . The input projection InProject embeds patch tokens into input embeddings \mathbf{h}^0 . Each AttnBlock consists of a multi-head self-attention layer, followed by a feed-forward network (FFN) and normalization layers. The output projection OutProject maps the output embeddings \mathbf{h}^L to the prediction $\hat{\mathbf{Y}}$, either directly [12, 11] or indirectly by first producing distributional parameters from which $\hat{\mathbf{Y}}$ is sampled [42]. We summarize the architectural features and training losses of each model in Appendix B.2.

3 Multi-Scale Finetuning of TSFM

3.1 Multi-Scale Effect on TSFM: A Causal View

As we discussed in Section 1, both time series data and TSFMs exhibit multi-scale properties. We take scale into account during TSFM finetuning and construct a Structural Causal Model (SCM) [28] as illustrated Figure 1 (b). The nodes denote the abstract data variables, and the directed edges denote the causality, i.e., cause \rightarrow effect. Denoting input context window data as X , scale as S , and prediction horizon window data as Y , we discuss the rationale for each link as follows:

$X \leftarrow S$. Given an observed recording of the context period, the input context series X is directly influenced by the scale S . Although corresponding to the same temporal range, X exhibits different temporal patterns and resolutions at different sampling rates.

$S \rightarrow M \leftarrow X$. We denote M as the activated knowledge within the pretrained TSFM’s knowledge space, conditioned on input context. $S \rightarrow M$ indicates that the scale of data activates the correspond-

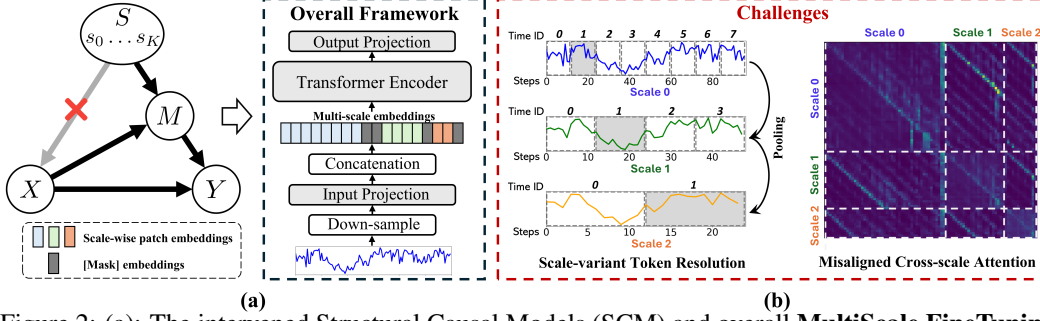


Figure 2: (a): The intervened Structural Causal Models (SCM) and overall **MultiScale FineTuning (MSFT)** framework, which directly model $P(Y|do(X))$; (b): Challenges in directly applying the framework. *Left*: Downsampling and patching process for constructing multi-scale sequences. Patch tokens at different scales have varying resolution and schematics. *Right*: Directly applying self-attention over multi-scale embeddings leads to biased cross-scale attention due to misaligned time id.

ing scale-specific knowledge in the TSFM. Meanwhile, $X \rightarrow M$ reflects that the TSFM activates context-specific knowledge with the input data X .

$X \rightarrow Y \leftarrow M$. This link represents that the model utilizes the activated knowledge M to generate predictions Y based on the lookback context data X .

It is evident that scale S is a confounder that induces spurious correlations between input context series (via $S \rightarrow X$) and activated knowledge of TSFM (via $S \rightarrow M$). The former captures the multi-scale properties of time series, while the latter corresponds to the multi-scale capabilities of TSFM. Scale S ultimately affects the forecasting of the prediction horizon via the backdoor path $X \leftarrow S \rightarrow M \rightarrow Y$. Naive finetuned forecaster for $P(Y|X)$ overlooks the impact of this backdoor path, learning forecasting only at the original scale. This oversight would mistakenly associate non-causal but positively correlated input context to forecast horizon in the original scale, resulting in problematic forecasting.

3.2 Causal Intervention via Backdoor Adjustment

Given this, we propose using $P(Y|do(X))$ as the new finetuned forecaster, which eliminates the confounding effect of S and captures the true causal relationship from X to Y . As the “physical” intervention is impossible, we apply the backdoor adjustment [27] to “virtually” realize $P(Y|do(X))$ by (1) blocking the link $S \rightarrow X$ and (2) S . As illustrated in Figure 2 (a, left), we have:

$$P(Y|do(X)) = \sum_s P(Y|X, S = s, M = g(X, s))P(s) \quad (2)$$

where g is a function to activate scale-specific knowledge of input. Grounded in this causal formulation, we design the **MultiScale FineTuning (MSFT)** framework to instantiate the intervention-based forecasting process shown in Equation 2. As shown in the right panel of Figure 2(a), the framework stratifies the confounder S by *down-sampling* the original time series into multiple scales. Each scale captures distinct statistical properties of the series and corresponds to a specific value $s \in S$.

Specifically, multi-scale series $\mathcal{S} = \{S_0, \dots, S_K\}$ is generated through the process described in Section 2. Each scale series S_i is segmented into scale-specific patch tokens $x_i \in \mathbb{R}^{N_i \times P}$, where N_i is the number of patches for scale i . The scale-specific input embeddings are computed by $h_i^0 = \text{InProject}(x_i)$. Following the design of masked encoder [9], the embeddings falling within the forecast horizon are replaced with the learnable [mask] embedding. The input embeddings from all scales are concatenated into a multi-scale sequence, $h_0 = \text{Concat}(h_0^0, h_1^0, \dots, h_K^0)$, which is then passed to the Transformer for processing.

3.3 Challenges

Although the framework of Figure 2(a) can be directly applied without initiation of $M = g(X, s)$, we argue that it leaves following challenges unaddressed. **First**, the token schematics and intra-scale dependencies vary significantly across scales. As shown in the left part of Figure 2(b), patch tokens at different scales exhibit distinct resolution and temporal schematics. When directly finetuning the

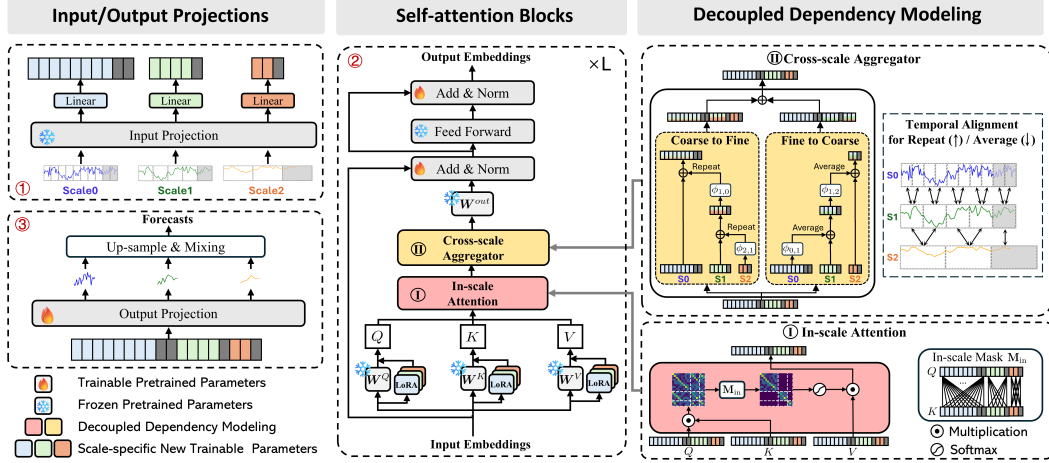


Figure 3: Complete design of MSFT based on the overall framework in Figure 2(a). ① Linear adapters are attached to the frozen input projection to learn scale-variant input embeddings. ② Self-attention layers incorporate scale-specific Lora and decoupled dependency modeling. ① In-scale attention employs in-scale masking, ensuring tokens attend only to others within the same scale. ② Cross-scale aggregators progressively fuse tokens across scales in two directions, ensuring correct temporal alignment between tokens. ③ Output projection generates separate predictions for each scale, which are then mixed by up-sampling and learned weights.

input projection layer over all scales, each scale inherently tends to learn its own specific intra-token patterns, which can lead to interference across scales and suboptimal performance. Moreover, the resolution discrepancy induces scale-inequivalent inter-token correlation, requiring the attention mechanism to capture scale-specific dynamics rather than assuming uniform interaction patterns.

Second, standard self-attention introduces misleading cross-scale dependencies due to mismatched time (position) indices. Since time indices are independently generated within each scale, tokens with the same index at different scales (shaded in gray in Figure 2(b)) correspond to different temporal ranges. When self-attention is directly applied over the concatenated multi-scale embedding sequence, attention scores across scales become biased: tokens attend more to others with the same time index, regardless of actual temporal relevance (see the right part of Figure 2(b)). This leads attention to capture spurious temporal correlations and attend to semantically irrelevant tokens.

Finally, the model generates distinct predictions at each scale, and effectively mixing multi-scale predictions remains a non-trivial challenge. Although cross-scale information is partially fused through attention, prior studies [41] have shown that explicitly combining multi-scale predictions improves forecasting performance. However, naively averaging predictions across scales fails to account for their semantic and temporal heterogeneity, potentially leading to suboptimal results.

4 Methodology

To address the aforementioned challenges, we propose **MSFT** to realize the high-level framework in Figure 2(a) as an effective multiscale finetuning strategy. Specifically, to **activate scale-specific knowledge**, we freeze the pretrained parameters and introduce scale-specific, parameter-efficient modules into the ① input projection and ② attention layers. To eliminate the cross-scale attention bias and correctly capture temporal correlations, we propose a **decoupled token dependency modeling** mechanism: ① in-scale self-attention captures within-scale dependencies, while ② cross-scale aggregators explicitly fuse information across scales, ensuring correct temporal alignment between tokens. Finally, we apply **multi-scale mixing** to the ③ output projection, combining scale-specific predictions with learned weights. Figure 3 illustrates our MSFT method.

Scale-specific Knowledge Activation. To address the problem of scale-variant token resolution, instead of directly finetuning the unified input projection layer across all scales, we freeze the pre-trained input projection and introduce a *scale-specific adapter* for each scale, implemented as a linear layer Linear_i . Now, the input embeddings of scale i is computed as $h_i^0 = \text{Linear}_i(\text{InProject}(x_i))$.

Conditioned on the pretrained embeddings, these adapters independently learn specific representations at variant resolutions, effectively avoiding interference across scales.

Similarly, to enhance the attention mechanism’s ability to capture scale-variant dynamics, we incorporate independent LoRA [13] modules for each scale. Specifically, we freeze the pretrained attention weight matrices, and the FFN block, and introduce a set of LoRA modules for each scale. Since both input embeddings and attention weights reflect scale-activated TSFM knowledge, this design serves as the implementation of g in Equation 2, enabling the activation of scale-specific knowledge M .

Decoupled Token Dependency Modeling. To ensure attention blocks capture the multi-scale embedding sequence’s correct dependencies, we decouple the token dependency modeling into two parts: within-scale and across-scale dependencies. Specifically, for tokens within the same scale, if they share the same resolution—dependencies, they can be directly learned via self-attention. Thus, we only apply an **in-scale attention mask** M_{in} to ensure that each token attends only to tokens from the same scale.

To aggregate the knowledge between tokens from different scales, we add a **cross-scale aggregator** after the attention operation. The aggregator consists of two branches, namely *coarse-to-fine* and *fine-to-coarse*, where temporal-aligned token-level information fusion is iteratively conducted between consecutive scales in two directions. First, since tokens at different scales correspond to varying resolutions, it is necessary to map embeddings to a shared space before fusion. To this end, following [29, 30], we adopt a linear mapping $\phi_{i,j}^l$ to project token embeddings from scale i to the embedding space of scale j in each layer l , where the mapped embeddings are defined as $\tilde{h}_{i,j}^l = \phi_{i,j}^l(h_i^l) = w_{i,j}^l h_i^l + b_{i,j}^l$.

Based on this mapping, token embeddings from one scale are projected to the adjacent scale and then fused according to their temporal alignment. We define the cross-scale token-wise fusion for the *coarse-to-fine* (C2F) and *fine-to-coarse* (F2C) branches as follows:

$$\text{C2F: } h_{i-1}^l = h_{i-1}^l + \text{Repeat}(\tilde{h}_{i,i-1}^l), \quad \text{for } i \in \{K, \dots, 1\} \quad (3)$$

$$\text{F2C: } h_{i+1}^l = h_{i+1}^l + \text{AvgPool}(\tilde{h}_{i,i+1}^l), \quad \text{for } i \in \{0, \dots, K-1\} \quad (4)$$

where $\text{Repeat}(\cdot)$ duplicates each coarse-scale token in $\tilde{h}_{i,i-1}^l$ along the sequence dimension to match the finer-scale resolution, based on their temporal correspondence. Conversely, $\text{AvgPool}(\cdot)$ aggregates groups of fine-scale tokens in $\tilde{h}_{i,i+1}^l$ by averaging them according to the downsampling factor, thereby aligning them to the coarser-scale resolution. Finally, the outputs from the two branches are combined by averaging their updated token embeddings. This decoupled two-stage design enables the model to capture temporal dependencies within each scale while effectively fusing complementary information across scales, leading to improved multi-scale temporal understanding.

Multi-scale Mixing. In the output projection, each scale independently predicts a forecasting horizon \hat{Y}_i based on its scale-specific tokens h_i^L from the final layer embedding h^L . The training objective is formulated as a weighted summation of the scale-wise forecasting losses $\mathcal{L}_{\text{pred},i}$ (e.g., MSE or NLL). Since different scales may exhibit varying forecasting abilities and contribute differently to the final performance, we assign a learnable weight w_i to each scale, corresponding to the prior $P(s)$ in Equation 2. The weights w_i are obtained by applying a softmax function over a set of learnable parameters during training: $\mathcal{L}_{\text{pred}} = \sum_{i=0}^{K+1} w_i \mathcal{L}_{\text{pred},i}$. During inference, we upsample the forecasting results from each new scale to the original temporal resolution. The final prediction \hat{Y} is computed as the weighted sum of the upsampled forecasts, using the same learned weights w_i . This weighted mixing strategy can be seen as ensembling [26], which helps mitigate overfitting on the original scale. Additional implementation details for different TSFM architectures are provided in Appendix B.2.

5 Related Work

5.1 Time Series Foundation Model

We focus our discussion solely on transformer-based TSFMs for TSF. Such TSFMs can be broadly categorized according to the backbone architecture. Encoder-only models like Moirai [42], Moment [12] and UniTS [11] use masked reconstruction for pretraining. Decoder-only models, such

as TimesFM [8], Lag-Llama [32], Timer [20], and Time-MoE [35] are pretrained by next-token prediction in an auto-regressive manner. Chronos [2], an encoder-decoder model, quantizes scaled time series values into discrete tokens and adopts the training objective originally developed for NLP. Despite the advancement of the field, existing TSFM research predominantly emphasizes pretraining and zero-shot performance. Although some studies [2, 12, 8, 20] mention naive finetuning methods, these attempts are limited compared to the efforts devoted to pretraining and zero-shot evaluation. We include a more detailed discussion in Appendix A.

5.2 Multi-scale modeling in time series forecasting

Multi-scale modeling has garnered growing attention in the TSF community. Existing works mostly involves down-sampling, where coarser scales are derived from the original series using pooling or convolution. Models are then designed to capture multi-scale characteristics from these different views. Pyraformer [18] constructs a pyramidal graph of different scales and employs a pyramid attention mechanism to extract multi-resolution representations. MICN [39] processes different scales separately through multiple branches with distinct convolution kernels and subsequently merges the outputs. Inspired by hierarchical forecasting, Scaleformer [34] and GPHT [21] iteratively refine the outputs from coarser to finer scales. TimeMixer [41] and TimeMixer++ [40] decompose each scale into seasonal and trend components, then integrate these components across multiple scales.

6 Experiments

We evaluate our proposed finetuning method, MSFT, on two prevalent TSF tasks: long sequence forecasting (LSF) and probabilistic forecasting (PF). For LSF, we experiment with three TSFMs: MOIRAI, MOMENT and UNITS. For PF, we focus solely on MOIRAI, as it is the only model capable of probabilistic forecasting. Our evaluation includes comparisons with both deep learning-based methods and other finetuning approaches applied to TSFMs. Detailed model configurations and experimental setups are provided in the Appendix B.

Table 1: Long sequence forecasting results, which are averaged across prediction lengths {96, 192, 336, 720}. Each TSFM shows its zero-shot performance (highlighted in gray) and results with different *finetuning methods*. The best finetuning results for each TSFM are highlighted in **bold**, while the global best results across all models are highlighted in **red**.

Method	ETTm1		ETTm2		ETTh1		ETTh2		Electricity		Weather	
	MSE	MAE	MSE	MAE	MSE	MAE	MSE	MAE	MSE	MAE	MSE	MAE
DLinear[2023]	0.403	0.419	0.350	0.401	0.456	0.452	0.559	0.515	0.212	0.365	0.265	0.317
PatchTST[2023]	0.387	0.400	0.281	0.326	0.469	0.455	0.387	0.407	0.216	0.304	0.259	0.281
iTransformer[2024a]	0.407	0.410	0.288	0.332	0.454	0.448	0.383	0.407	0.178	0.270	0.258	0.278
TimeMixer[2024]	0.381	0.395	0.275	0.323	0.447	0.440	0.364	0.395	0.182	0.272	0.240	0.271
SimpleTM [2025]	0.381	0.396	0.275	0.322	0.422	0.428	0.353	0.391	0.166	0.260	0.243	0.271
MOIRAI _{Small}	0.448	0.409	0.300	0.341	0.416	0.428	0.355	0.381	0.233	0.320	0.268	0.279
+ Full finetuning	0.367	0.382	0.273	0.316	0.415	0.429	0.352	0.378	0.193	0.279	0.228	0.254
+ Linear probing	0.388	0.392	0.295	0.337	0.414	0.427	0.354	0.380	0.212	0.299	0.237	0.260
+ Prompt tuning	0.384	0.391	0.292	0.334	0.414	0.428	0.354	0.381	0.217	0.304	0.235	0.258
+ LoRA	0.370	0.383	0.272	0.314	0.414	0.427	0.354	0.380	0.192	0.279	0.225	0.252
+ AdaLoRA	0.381	0.386	0.273	0.319	0.414	0.427	0.354	0.380	0.191	0.279	0.226	0.252
+ MSFT	0.353	0.377	0.250	0.301	0.412	0.426	0.349	0.375	0.187	0.275	0.216	0.248
MOIRAI _{Base}	0.381	0.388	0.281	0.326	0.412	0.424	0.356	0.388	0.188	0.274	0.246	0.265
+ Full finetuning	0.368	0.371	0.258	0.307	0.409	0.424	0.357	0.384	0.173	0.263	0.232	0.258
+ Linear probing	0.388	0.387	0.277	0.319	0.409	0.424	0.356	0.387	0.182	0.269	0.229	0.253
+ Prompt tuning	0.378	0.386	0.280	0.325	0.412	0.423	0.360	0.387	0.183	0.271	0.230	0.255
+ LoRA	0.361	0.371	0.259	0.308	0.409	0.423	0.358	0.384	0.173	0.263	0.230	0.258
+ AdaLoRA	0.359	0.371	0.258	0.307	0.410	0.423	0.356	0.384	0.173	0.264	0.236	0.260
+ MSFT	0.332	0.369	0.247	0.305	0.407	0.422	0.352	0.383	0.169	0.260	0.213	0.245
MOMENT	-	-	-	-	-	-	-	-	-	-	-	-
+ Full finetuning	0.352	0.380	0.260	0.320	0.425	0.440	0.347	0.394	0.224	0.311	0.336	0.310
+ Linear probing	0.355	0.381	0.261	0.321	0.429	0.441	0.347	0.395	0.226	0.313	0.338	0.312
+ Prompt tuning	0.356	0.381	0.261	0.320	0.427	0.440	0.348	0.395	0.226	0.312	0.336	0.310
+ LoRA	0.356	0.381	0.260	0.320	0.425	0.439	0.347	0.395	0.225	0.312	0.335	0.309
+ AdaLoRA	0.355	0.381	0.259	0.319	0.426	0.440	0.347	0.394	0.224	0.311	0.336	0.311
+ MSFT	0.344	0.377	0.255	0.316	0.422	0.436	0.345	0.392	0.221	0.309	0.332	0.307
UNITS	0.713	0.553	0.321	0.355	0.527	0.491	0.406	0.418	0.432	0.488	0.291	0.313
+ Full finetuning	0.395	0.405	0.297	0.338	0.442	0.435	0.386	0.409	0.190	0.283	0.257	0.283
+ Linear probing	0.399	0.409	0.301	0.343	0.445	0.437	0.392	0.412	0.200	0.291	0.274	0.293
+ Prompt tuning	0.431	0.430	0.299	0.341	0.438	0.433	0.386	0.405	0.191	0.287	0.247	0.276
+ LoRA	0.393	0.405	0.296	0.338	0.437	0.434	0.384	0.407	0.188	0.282	0.250	0.279
+ MSFT	0.390	0.403	0.288	0.334	0.434	0.430	0.380	0.405	0.184	0.279	0.242	0.273

Table 2: Probabilistic forecasting results. The best finetuning results for each TSFM are highlighted in **bold**, while the global best results are highlighted in **red**. See Table 11 for full results.

Method	Electricity		Solar		Weather		Istanbul Traffic		Turkey Power	
	CRPS	MSIS	CRPS	MSIS	CRPS	MSIS	CRPS	MSIS	CRPS	MSIS
DeepAR[2020]	0.065	6.893	0.431	11.181	0.132	21.651	0.108	4.094	0.066	13.520
TFT[2021]	0.050	6.278	0.446	8.057	0.043	7.791	0.110	4.057	0.039	7.943
PatchTST[2023]	0.052	5.744	0.518	8.447	0.059	7.759	0.112	3.813	0.054	8.978
TiDE[2023]	0.048	5.672	0.420	13.754	0.054	8.095	0.110	4.752	0.046	8.579
MOIRAI _{Small}	0.072	7.999	0.471	8.425	0.049	5.236	0.173	5.937	0.048	7.127
+ Full finetuning	0.055	6.009	0.395	6.947	0.039	4.477	0.151	6.735	0.040	6.887
+ Linear probing	0.062	6.438	0.369	5.865	0.049	4.785	0.154	4.645	0.047	6.912
+ Prompt tuning	0.066	6.595	0.421	6.936	0.050	4.901	0.154	4.733	0.045	7.042
+ LoRA	0.064	6.753	0.372	6.582	0.039	4.386	0.154	4.753	0.042	7.051
+ AdaLoRA	0.064	6.892	0.366	8.015	0.040	4.496	0.152	4.670	0.041	7.127
+ MSFT	0.047	5.327	0.353	7.706	0.036	4.178	0.141	4.447	0.038	6.810
MOIRAI _{Base}	0.055	6.172	0.419	7.011	0.041	5.136	0.116	4.461	0.040	6.766
+ Full finetuning	0.049	5.414	0.188	4.292	0.038	5.282	0.120	7.272	0.036	6.712
+ Linear probing	0.055	5.951	0.379	5.645	0.039	4.544	0.104	3.736	0.042	7.259
+ Prompt tuning	0.054	6.024	0.412	6.885	0.040	5.274	0.105	3.987	0.040	6.698
+ LoRA	0.051	5.651	0.382	6.745	0.037	4.904	0.113	4.752	0.036	6.744
+ AdaLoRA	0.054	5.937	0.383	8.825	0.038	4.802	0.110	3.895	0.037	6.762
+ MSFT	0.046	5.199	0.142	3.464	0.035	4.603	0.098	3.685	0.034	6.419

6.1 Long Sequence Forecasting

Setup. We conduct our experiments on a subset of the widely-used long sequence forecasting benchmark [44]. This subset is identical to the one used in Moirai [42] for LSF experiments and is not included in the pretraining data of TSFMs. Each dataset involves predictions at four different lengths, with the model is finetuned separately for each prediction length. We evaluate the performance using Mean Squared Error (MSE) and Mean Absolute Error (MAE).

Results. As shown in Table 1, MSFT consistently enhances the forecasting performance of TSFMs. Across all models, MSFT outperforms other finetuning methods that use only the original scale, consistently delivering the best finetuned results. For MOIRAI_{Small} and MOIRAI_{Base}, MSFT further improves their forecasting accuracy over their solid zero-shot performance, achieving competitive results across all datasets, with 10 out of 12 metrics showing the best performance. Notably, MSFT substantially improves MOIRAI’s finetuned performance on minutely-level datasets. Compared to full finetuning, it achieves 6.8% lower MSE in ETTm1, 6.3% lower MSE in ETTm2 and 6.7% lower MSE in Weather. In contrast, the improvement brought by MSFT on hourly datasets are relatively smaller compared to minute-level datasets. This discrepancy can be explained by the richer multi-scale patterns present in minute-level data, which MSFT can effectively leverage. For MOMENT, the improvements brought by MSFT are generally less pronounced compared to MOIRAI and UNITS. This can be attributed its pretraining with fixed context lengths, which limits their ability to extract information from new scales of varying lengths. Despite these differences, MSFT exhibit superior finetuned performance across diverse models and datasets, demonstrating its generalizability.

6.2 Probabilistic Forecasting

Setup. We evaluate on six datasets spanning various domains, using the rolling evaluation setup described in Moirai [42]. The test set comprises the final time steps, segmented into multiple non-overlapping evaluation windows. The length of the prediction window and the number of rolling evaluations are tailored for each dataset based on its frequency (see Table 5 for details). For performance evaluation, we report the Continuous Ranked Probability Score (CRPS) and Mean Scaled Interval Score (MSIS) metrics.

Results. Experimental results in Table 2 demonstrate that MSFT consistently delivers superior performance across all datasets. Building upon the strong zero-shot performance, MOIRAI_{Base} achieves the best results for nearly all the datasets. MSFT provides consistent improvements over other finetuning methods, achieving an additional 24.4 % CPRS relative reduction in Solar and 18.3 % CPRS relative reduction in Istanbul Traffic compared to full finetuning. A similar trend is also observed in the small model, demonstrating that our multi-scale modeling method can effectively enhance the fine-tuned performance of probabilistic forecasting.

Table 3: Ablation study on three LSF datasets using MOIRAI_{Small}.

	InProject		Attention		In-scale Mask	X-scale Aggre.		Mixing		ETTm1		ETTm2		Weather		Avg Diff	
	Scale	Shared	Scale	Shared		C2F	F2C	Avg.	Weighted	MSE	MAE	MSE	MAE	MSE	MAE	MSE	MAE
①			✓		✓	✓	✓		✓	0.361	0.379	0.253	0.305	0.219	0.252	0.005	0.003
②		✓		✓	✓	✓	✓		✓	0.359	0.378	0.252	0.304	0.218	0.249	0.003	0.002
③	✓				✓	✓	✓		✓	0.372	0.383	0.256	0.308	0.224	0.256	0.011	0.007
④	✓			✓	✓	✓	✓		✓	0.360	0.381	0.254	0.306	0.221	0.254	0.005	0.005
⑤	✓		✓		✓				✓	0.370	0.383	0.256	0.307	0.223	0.255	0.010	0.006
⑥	✓		✓		✓				✓	0.362	0.381	0.254	0.304	0.220	0.252	0.006	0.004
⑦	✓		✓		✓		✓		✓	0.356	0.379	0.253	0.304	0.218	0.251	0.003	0.003
⑧	✓		✓		✓				✓	0.359	0.380	0.253	0.303	0.219	0.252	0.004	0.003
⑨	✓		✓		✓	✓	✓			0.360	0.379	0.268	0.312	0.225	0.251	0.011	0.005
⑩	✓		✓		✓	✓	✓	✓		0.380	0.385	0.254	0.310	0.219	0.252	0.008	0.007
MSFT	✓		✓		✓	✓	✓	✓		0.353	0.377	0.250	0.301	0.216	0.248	-	-

6.3 Model Analysis

To fully understand MSFT, we conduct model analysis using the MOIRAI_{Small} model on three LSF datasets, selected for its strong zero-shot performance and relatively low training cost. Due to page limits, we present the analysis of down-sampling approaches, down-sampling factors, detailed attention analysis, and visualizations in the Appendix C. We also discuss the potential application of MSFT to decoder-based structures and its limitation in Appendix D.

Ablation Study. Ablations ① to ④ examine the effectiveness of scale-specific knowledge activation. For both input projection and attention, either freezing (①, ③) or finetuning shared weights (②, ④) yields inferior performance to using scale-specific modules, with freezing causing larger performance drops. Among the two, attention has a greater impact than input projection, highlighting its critical role in capturing temporal dependencies.

Ablations ⑤ to ⑧ evaluate the effect of each component in decoupled dependency modeling. In ⑤, we remove cross-scale aggregators and only retain in-scale attention masking. Without cross-scale modeling, the performance suffers a significant decline. In ⑥ and ⑦, we ablate the coarse-to-fine and fine-to-coarse branches, respectively. Both cases lead to performance drops, with the coarse-to-fine branch showing a stronger impact. In ⑧, we completely remove decoupled dependency modeling, capturing dependency directly via attention on the concatenated multi-scale sequence. This approach leads to misaligned cross-scale interactions and further degrades performance.

Finally, we assess the impact of multi-scale mixing. In ⑨, we disable prediction mixing, only using the original scale for prediction. In ⑩, we aggregate the multi-scale predictions by averaging. Both approaches result in lower performance compared to our full model.

Effect of Number of New Scales. As shown in Figure 4, increasing the number of new scales K initially reduces errors. However, beyond a certain point, performance plateaus or declines, likely due to overly coarse predictions with few tokens disrupting multi-scale modeling. Our results indicate that setting K to 2 or 3 achieves the best balance.

Attention Analysis. Figure 5 shows the attention score heatmaps of three attention strategies. In (a), direct attention (Ablation ⑧) exhibits spurious temporal dependencies, with attention scores biased toward tokens sharing the same time indices. In (b), we align time indices during attention, ensuring that cross-scale tokens corresponding to the same temporal region share identical time indices. While this approach produces "correct" attention patterns, it is limited to RoPE and performs worse than our method (see Appendix C for details). In (c), our in-scale masking strategy eliminates misleading cross-scale attention, focusing on accurate within-scale dependency modeling.

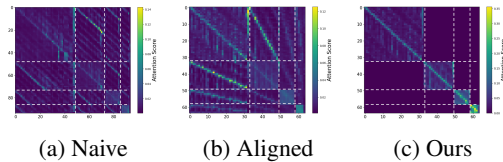
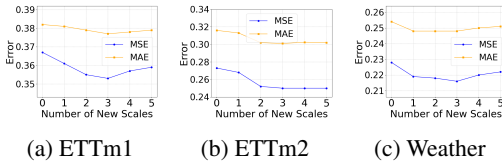


Figure 4: LSF accuracy w.r.t. number of scales

Figure 5: Attention heatmaps of various methods

7 Conclusion

We introduce MSFT, a multi-scale finetuning strategy for encoder-based TSFMs. From a causal view, we highlight the limitations of naive finetuning and propose to use multi-scale modeling as backdoor adjustment to mitigate the confounding effect of scale. By using concatenated multi-scale sequence as input, applying simple scale-specific model modifications, and employing decoupled dependency modeling, our method effectively aggregates multi-scale information and improves the forecasting performance. Our experiments show that MSFT not only significantly enhances the performance of the original foundation models but also surpasses other state-of-the-art models trained from scratch.

Acknowledgments and Disclosure of Funding

This research is part of the programme DesCartes and is supported by the National Research Foundation, Prime Minister’s Office, Singapore under its Campus for Research Excellence and Technological Enterprise (CREATE) programme.

References

- [1] Alexander Alexandrov, Konstantinos Benidis, Michael Bohlke-Schneider, Valentin Flunkert, Jan Gasthaus, Tim Januschowski, Danielle C. Maddix, Syama Rangapuram, David Salinas, Jasper Schulz, Lorenzo Stella, Ali Caner Trkmen, and Yuyang Wang. 2020. GluonTS: Probabilistic and Neural Time Series Modeling in Python. *Journal of Machine Learning Research* 21, 116 (2020), 1–6. <http://jmlr.org/papers/v21/19-820.html>
- [2] Abdul Fatir Ansari, Lorenzo Stella, Caner Turkmen, Xiyuan Zhang, Pedro Mercado, Huibin Shen, Oleksandr Shchur, Syama Syndar Rangapuram, Sebastian Pineda Arango, Shubham Kapoor, Jasper Zschiegner, Danielle C. Maddix, Michael W. Mahoney, Kari Torkkola, Andrew Gordon Wilson, Michael Bohlke-Schneider, and Yuyang Wang. 2024. Chronos: Learning the Language of Time Series. *Transactions on Machine Learning Research* (2024).
- [3] Abdelhakim Benezhab, Vasilii Feofanov, Giuseppe Paolo, Albert Thomas, Maurizio Filippone, and Balsz Kgl. 2025. AdaPTS: Adapting Univariate Foundation Models to Probabilistic Multivariate Time Series Forecasting. arXiv:2502.10235 [stat.ML] <https://arxiv.org/abs/2502.10235>
- [4] Hui Chen, Viet Luong, Lopamudra Mukherjee, and Vikas Singh. 2025. SimpleTM: A Simple Baseline for Multivariate Time Series Forecasting. In *The Thirteenth International Conference on Learning Representations*.
- [5] Peng Chen, Yingying ZHANG, Yunyao Cheng, Yang Shu, Yihang Wang, Qingsong Wen, Bin Yang, and Chenjuan Guo. 2024. Pathformer: Multi-scale Transformers with Adaptive Pathways for Time Series Forecasting. In *The Twelfth International Conference on Learning Representations*.
- [6] Abhimanyu Das, Matthew Faw, Rajat Sen, and Yichen Zhou. 2024. In-context Fine-tuning for Time-series Foundation Models.
- [7] Abhimanyu Das, Weihao Kong, Andrew Leach, Shaan K Mathur, Rajat Sen, and Rose Yu. 2023. Long-term Forecasting with TiDE: Time-series Dense Encoder. *Transactions on Machine Learning Research* (2023).
- [8] Abhimanyu Das, Weihao Kong, Rajat Sen, and Yichen Zhou. 2024. A decoder-only foundation model for time-series forecasting. In *Forty-first International Conference on Machine Learning*.
- [9] Jacob Devlin, Ming-Wei Chang, Kenton Lee, and Kristina Toutanova. 2018. Bert: Pre-training of deep bidirectional transformers for language understanding. In *Proceedings of the 2019 Conference of the North American Chapter of the Association for Computational Linguistics: Human Language Technologies*.

- [10] Vijay Ekambaram, Arindam Jati, Nam H Nguyen, Pankaj Dayama, Chandra Reddy, Wesley M Gifford, and Jayant Kalagnanam. 2024. Ttms: Fast multi-level tiny time mixers for improved zero-shot and few-shot forecasting of multivariate time series. *arXiv preprint arXiv:2401.03955* 8 (2024), 22.
- [11] Shanghua Gao, Teddy Koker, Owen Queen, Thomas Hartvigsen, Theodoros Tsiligkaridis, and Marinka Zitnik. 2024. UniTS: A Unified Multi-Task Time Series Model. In *The Thirty-eighth Annual Conference on Neural Information Processing Systems*.
- [12] Mononito Goswami, Konrad Szafer, Arjun Choudhry, Yifu Cai, Shuo Li, and Artur Dubrawski. 2024. MOMENT: A Family of Open Time-series Foundation Models. In *International Conference on Machine Learning*.
- [13] Edward J Hu, yelong shen, Phillip Wallis, Zeyuan Allen-Zhu, Yanzhi Li, Shean Wang, Lu Wang, and Weizhu Chen. 2022. LoRA: Low-Rank Adaptation of Large Language Models. In *International Conference on Learning Representations*.
- [14] Taesung Kim, Jinhee Kim, Yunwon Tae, Cheonbok Park, Jang-Ho Choi, and Jaegul Choo. 2022. Reversible Instance Normalization for Accurate Time-Series Forecasting against Distribution Shift. In *International Conference on Learning Representations*.
- [15] Ananya Kumar, Aditi Raghunathan, Robbie Matthew Jones, Tengyu Ma, and Percy Liang. 2022. Fine-Tuning can Distort Pretrained Features and Underperform Out-of-Distribution. In *International Conference on Learning Representations*.
- [16] Guokun Lai, Wei-Cheng Chang, Yiming Yang, and Hanxiao Liu. 2018. Modeling Long- and Short-Term Temporal Patterns with Deep Neural Networks. In *The 41st International ACM SIGIR Conference on Research & Development in Information Retrieval (SIGIR '18)*. 95–104.
- [17] Bryan Lim, Sercan Ö Arık, Nicolas Loeff, and Tomas Pfister. 2021. Temporal fusion transformers for interpretable multi-horizon time series forecasting. *International Journal of Forecasting* 37, 4 (2021), 1748–1764.
- [18] Shizhan Liu, Hang Yu, Cong Liao, Jianguo Li, Weiyao Lin, Alex X. Liu, and Schahram Dustdar. 2022. Pyraformer: Low-Complexity Pyramidal Attention for Long-Range Time Series Modeling and Forecasting. In *International Conference on Learning Representations*.
- [19] Yong Liu, Tengge Hu, Haoran Zhang, Haixu Wu, Shiyu Wang, Lintao Ma, and Mingsheng Long. 2024. iTransformer: Inverted Transformers Are Effective for Time Series Forecasting. In *The Twelfth International Conference on Learning Representations*.
- [20] Yong Liu, Haoran Zhang, Chenyu Li, Xiangdong Huang, Jianmin Wang, and Mingsheng Long. 2024. Timer: Generative Pre-trained Transformers Are Large Time Series Models. In *Forty-first International Conference on Machine Learning*.
- [21] Zhiding Liu, Jiqian Yang, Mingyue Cheng, Yucong Luo, and Zhi Li. 2024. Generative Pretrained Hierarchical Transformer for Time Series Forecasting. In *Proceedings of the 30th ACM SIGKDD Conference on Knowledge Discovery and Data Mining (KDD '24)*. 2003–2013.
- [22] Sourab Mangrulkar, Sylvain Gugger, Lysandre Debut, Younes Belkada, Sayak Paul, and Benjamin Bossan. 2022. PEFT: State-of-the-art Parameter-Efficient Fine-Tuning methods. <https://github.com/huggingface/peft>.
- [23] Michael C Mozer. 1991. Induction of Multiscale Temporal Structure. In *Advances in Neural Information Processing Systems*, J. Moody, S. Hanson, and R.P. Lippmann (Eds.), Vol. 4. Morgan-Kaufmann.
- [24] Jishnu Mukhoti, Yarin Gal, Philip Torr, and Puneet K. Dokania. 2024. Fine-tuning can cripple your foundation model; preserving features may be the solution. *Transactions on Machine Learning Research* (2024). Featured Certification.
- [25] Yuqi Nie, Nam H Nguyen, Phanwadee Sinthong, and Jayant Kalagnanam. 2023. A Time Series is Worth 64 Words: Long-term Forecasting with Transformers. In *The Eleventh International Conference on Learning Representations*.

- [26] Boris N. Oreshkin, Dmitri Carpow, Nicolas Chapados, and Yoshua Bengio. 2020. N-BEATS: Neural basis expansion analysis for interpretable time series forecasting. In *International Conference on Learning Representations*. <https://openreview.net/forum?id=r1ecqn4YwB>
- [27] Judea Pearl. 2014. Interpretation and identification of causal mediation. *Psychological methods* 19, 4 (2014), 459.
- [28] Judea Pearl. 2016. *Causal inference in statistics: a primer*. John Wiley & Sons.
- [29] Ethan Perez, Florian Strub, Harm de Vries, Vincent Dumoulin, and Aaron Courville. 2018. FiLM: visual reasoning with a general conditioning layer (AAAI’18/IAAI’18/EAAI’18). AAAI Press, 10 pages.
- [30] Quang Pham, Chenghao Liu, and Steven Hoi. 2021. Dualnet: Continual learning, fast and slow. *Advances in Neural Information Processing Systems* 34 (2021), 16131–16144.
- [31] Colin Raffel, Noam Shazeer, Adam Roberts, Katherine Lee, Sharan Narang, Michael Matena, Yanqi Zhou, Wei Li, and Peter J Liu. 2020. Exploring the limits of transfer learning with a unified text-to-text transformer. *Journal of machine learning research* 21, 140 (2020), 1–67.
- [32] Kashif Rasul, Arjun Ashok, Andrew Robert Williams, Arian Khorasani, George Adamopoulos, Rishika Bhagwatkar, Marin Biloš, Hena Ghonia, Nadhir Hassen, Anderson Schneider, Sahil Garg, Alexandre Drouin, Nicolas Chapados, Yuriy Nevmyvaka, and Irina Rish. 2023. Lag-Llama: Towards Foundation Models for Time Series Forecasting. In *R0-FoMo: Robustness of Few-shot and Zero-shot Learning in Large Foundation Models*.
- [33] David Salinas, Valentin Flunkert, Jan Gasthaus, and Tim Januschowski. 2020. DeepAR: Probabilistic forecasting with autoregressive recurrent networks. *International Journal of Forecasting* 36, 3 (2020), 1181–1191.
- [34] Mohammad Amin Shabani, Amir H. Abdi, Lili Meng, and Tristan Sylvain. 2023. Scaleformer: Iterative Multi-scale Refining Transformers for Time Series Forecasting. In *The Eleventh International Conference on Learning Representations*.
- [35] Xiaoming Shi, Shiyu Wang, Yuqi Nie, Dianqi Li, Zhou Ye, Qingsong Wen, and Ming Jin. 2025. Time-MoE: Billion-Scale Time Series Foundation Models with Mixture of Experts. In *The Thirteenth International Conference on Learning Representations*.
- [36] Jianlin Su, Murtadha Ahmed, Yu Lu, Shengfeng Pan, Wen Bo, and Yunfeng Liu. 2024. RoFormer: Enhanced transformer with Rotary Position Embedding. *Neurocomput.* 568, C (March 2024), 12 pages.
- [37] Artur Trindade. 2015. ElectricityLoadDiagrams20112014. UCI Machine Learning Repository. DOI: <https://doi.org/10.24432/C58C86>.
- [38] Ashish Vaswani, Noam Shazeer, Niki Parmar, Jakob Uszkoreit, Llion Jones, Aidan N Gomez, Łukasz Kaiser, and Illia Polosukhin. 2017. Attention is All you Need. In *Advances in Neural Information Processing Systems*, I. Guyon, U. Von Luxburg, S. Bengio, H. Wallach, R. Fergus, S. Vishwanathan, and R. Garnett (Eds.), Vol. 30.
- [39] Huiqiang Wang, Jian Peng, Feihu Huang, Jince Wang, Junhui Chen, and Yifei Xiao. 2023. MICN: Multi-scale Local and Global Context Modeling for Long-term Series Forecasting. In *The Eleventh International Conference on Learning Representations*.
- [40] Shiyu Wang, Jiawei LI, Xiaoming Shi, Zhou Ye, Baichuan Mo, Wenze Lin, Ju Shengtong, Zhixuan Chu, and Ming Jin. 2025. TimeMixer++: A General Time Series Pattern Machine for Universal Predictive Analysis. In *The Thirteenth International Conference on Learning Representations*.
- [41] Shiyu Wang, Haixu Wu, Xiaoming Shi, Tengge Hu, Huakun Luo, Lintao Ma, James Y. Zhang, and JUN ZHOU. 2024. TimeMixer: Decomposable Multiscale Mixing for Time Series Forecasting. In *The Twelfth International Conference on Learning Representations*.

- [42] Gerald Woo, Chenghao Liu, Akshat Kumar, Caiming Xiong, Silvio Savarese, and Doyen Sahoo. 2024. Unified Training of Universal Time Series Forecasting Transformers. In *Forty-first International Conference on Machine Learning*.
- [43] Haixu Wu, Tengge Hu, Yong Liu, Hang Zhou, Jianmin Wang, and Mingsheng Long. 2023. TimesNet: Temporal 2D-Variation Modeling for General Time Series Analysis. In *The Eleventh International Conference on Learning Representations*.
- [44] Haixu Wu, Jiehui Xu, Jianmin Wang, and Mingsheng Long. 2021. Autoformer: Decomposition transformers with auto-correlation for long-term series forecasting. *Advances in Neural Information Processing Systems* 34 (2021), 22419–22430.
- [45] Ailing Zeng, Muxi Chen, Lei Zhang, and Qiang Xu. 2023. Are transformers effective for time series forecasting?. In *Proceedings of the AAAI conference on artificial intelligence*, Vol. 37. 11121–11128.
- [46] Jiawen Zhang, Shun Zheng, Xumeng Wen, Xiaofang Zhou, Jiang Bian, and Jia Li. 2024. ElasTST: Towards Robust Varied-Horizon Forecasting with Elastic Time-Series Transformer. In *The Thirty-eighth Annual Conference on Neural Information Processing Systems*.
- [47] Qingru Zhang, Minshuo Chen, Alexander Bukharin, Pengcheng He, Yu Cheng, Weizhu Chen, and Tuo Zhao. 2023. Adaptive Budget Allocation for Parameter-Efficient Fine-Tuning. In *The Eleventh International Conference on Learning Representations*.
- [48] Yitian Zhang, Liheng Ma, Soumyasundar Pal, Yingxue Zhang, and Mark Coates. 2024. Multi-resolution Time-Series Transformer for Long-term Forecasting. In *Proceedings of The 27th International Conference on Artificial Intelligence and Statistics*. PMLR, 4222–4230.
- [49] Haoyi Zhou, Shanghang Zhang, Jieqi Peng, Shuai Zhang, Jianxin Li, Hui Xiong, and Wancai Zhang. 2021. Informer: Beyond Efficient Transformer for Long Sequence Time-Series Forecasting. In *The Thirty-Fifth AAAI Conference on Artificial Intelligence, AAAI 2021, Virtual Conference*, Vol. 35. AAAI Press, 11106–11115.

A Detailed Related Works

A.1 Time Series Foundation Model

In this section, we further discuss related works involved TSFM finetuning. Some TSFMs conduct basic experiments in their original papers to show the effect of naive finetuning. For instance, Moment [12] applies linear probing and reports the corresponding results in their main experiments. Chronos [2] and Timer [20] apply full finetuning, with improvements over zero-shot performance on their respective benchmarks. TimesFM [8] tunes the input and output residual blocks on ETT datasets.

Notably, some recent studies explore specialized finetuning methods for TSFMs. UniTS [11] introduces a prompt tuning strategy, and [6] employs in-context tuning to TimesFM. However, both methods are tailored to their own model architectures and rely on specialized pretraining designs, which limits their generalizability and plug-and-play applicability. [3] inserts adapters on Moment to adapt this univariate TSFM for multivariate probabilistic forecasting. However, this approach is restricted to this specific application, rather than serving as a general finetuning method applicable to various models or forecasting tasks. This gap underscores the need for more general, effective, and modular finetuning strategies for TSFMs.

A.2 Multi-scale modeling

Besides the down-sampling-based methods discussed in Section 5.2, there is another strategy *multi-patch*, which applies specifically to patch-based TSTs. Here, multiple patch sizes are used to segment the time series into tokens in different resolutions. Pathformer [5] applies layer-by-layer routing to select patch sizes and aggregate the outputs from multiple scales. MTST [48] proposes a multi-branch architecture for modeling diverse temporal patterns at different resolutions. ElasTST [46] leverages a shared transformer backbone with tunable RoPE for multi-scale patch assembly. However, this line of methods requires the model to be compatible with multiple patch sizes, which is not feasible for most TSFMs.

Despite these efforts to incorporate multi-scale features, our proposed method exhibits two key differences from current approaches. First, most of these models are trained from scratch on a single dataset, leaving open questions about how to effectively leverage pretrained TSFMs for multi-scale modeling. Our method is the first to explore multi-scale modeling directly on pretrained TSFMs. Second, existing methods primarily perform cross-scale aggregation at the feature or time series level, whereas our approach achieves this at the token level.

B Implementation Details

B.1 Dataset details

For long sequence forecasting (LSF), we conduct experiments on six well-established datasets, including the ETT datasets (ETTh1, ETTh2, ETTm1, ETTm2) [49], Weather [44], and Electricity [44]. We note that these datasets are not included in the pretraining datasets of the TSFMs we evaluated. The key properties of these LSF datasets are detailed in Table 4.

Table 4: Summary of datasets used in the long sequence forecasting evaluation.

Task	Dataset	Variate	Dataset Size	Predict Length	Frequency	Information
Long Sequence Forecasting	ETTh1	7	17420	{96, 192, 336, 720}	Hourly	Temperature
	ETTh2	7	17420	{96, 192, 336, 720}	Hourly	Temperature
	ETTm1	7	69680	{96, 192, 336, 720}	15 min	Temperature
	ETTm2	7	69680	{96, 192, 336, 720}	15 min	Temperature
	Electricity	321	26304	{96, 192, 336, 720}	Hourly	Electricity
	Weather	21	52696	{96, 192, 336, 720}	10 min	Weather

Following Moirai [42], we use 5 out-of-distribution datasets for probabilistic forecasting: Electricity [37], Solar-Power [16], Jena Weather, Istanbul Traffic², and Turkey Power³. Detailed descriptions of these datasets are provided in Table 5.

Table 5: Summary of datasets used in the probabilistic forecasting evaluation setting.

Task	Dataset	Variate	Dataset Size	Predict Length	Rolling Evaluation	Frequency	Information
Probabilistic Forecasting	Electricity	321	26304	24	7	H	Energy
	Solar	137	8760	24	7	H	Energy
	Weather	21	52696	144	7	10T	Climate
	Istanbul Traffic	3	14244	24	7	H	Transport
	Turkey Power	18	26304	24	7	H	Energy

B.2 Encoder-based TSFMs

In this section, we describe the architectural details and training objectives of each encoder-based TSFM used in our experiments. Table 6 summarizes the fundamental characteristics of the models based on their origin setup.

Table 6: Summary of encoder-based time series foundation models.

Feature	Moirai	Moment	UNITS
Citation	Woo et al., 2024	Goswami et al., 2024	Gao et al., 2024
Base Architecture	Naive Encoder	T5 Encoder	Modified Encoder
Params	<i>Small</i> : 14M, <i>Base</i> : 91M	40M	3.4M
Open Source	✓	✓	✓
Evaluation Tasks	Point Forecasting, Probabilistic Forecasting	Point Forecasting, Classification, Anomaly detection, Imputation	Point Forecasting, Classification, Anomaly detection, Imputation
Layer	<i>Small</i> : 6, <i>Base</i> : 12	8	3
d_{model}	<i>Small</i> : 384, <i>Base</i> : 768	512	128
Patch Size	[8, 16, 32, 64, 128]	8	16
Context Length	1000-5000	512	96
Position Embedding	RoPE [36]	Sinusoidal	Learnable Additive PE

Moirai Moirai [42] is one of the pioneering TSFMs for universal time series forecasting based on a masked encoder architecture. It segments single-dimensional time series (a variate) into patch tokens and can be extended to multivariate setup by flattening multiple variate into a single sequence. Moirai employs multi patch size projection layers in both input and output projections, allowing it to effectively handle data with varying frequencies. In the attention blocks, it encodes the temporal position of tokens using Rotary Positional Encoding (RoPE) [36], and encodes simple variate correlation by using binary attention biases to indicate whether two tokens belong to the same variate or not. The model produces distribution parameters for a mixture distribution over the predictive horizon. The training objective is to minimize the negative log-likelihood (NLL). During inference, predictions of horizon are obtained by sampling from the predictive distribution. Point forecasts can be derived by taking the median from the samples. In our experiments, we use the univariate mode of Moirai, encoding different scales using distinct variate indices.

Moment Moment [12] is a suite of open-source foundation models designed for versatile time-series analysis tasks. Moment follows channel independence assumption and leverages a T5[31] encoder architecture enhanced with sinusoidal positional encoding to effectively capture temporal dependencies within time series. Distinctively, during the forecasting fine-tuning phase, MOMENT utilizes the entire context series as input to directly get prediction results, diverging from traditional masked reconstruction methods commonly employed in pretraining. The model’s forecasting head comprises a flatten operation followed by a linear layer, and it is trained using the MSE loss function. Due to the computational resource constraints associated with finetuning and the large scale of the models, we employ Moment (Small) for our experiments.

²<https://www.kaggle.com/datasets/leonardo00/istanbul-traffic-index>

³<https://www.kaggle.com/datasets/dharanikra/electrical-power-demand-in-turkey>

UNITS UNITS is originally designed for multi-tasks learning with specific task prompts. The transformer encoder is composed of multiple UNITS Blocks and ultimately processed through the GEN Tower to generate the final predictions. Specifically, within each UNITS Block, the data sequentially passes through Time Self-attention, Variable Self-attention, and Dynamic FFN. Each of these modules is followed by a Gate Module, which enhances the model’s generalization capability in multi-task learning by dynamically scaling the feature vectors. Time Self-attention and Variable Self-attention compute attention scores along the time and variable dimensions, respectively, while the Dynamic FFN dynamically adjusts the shape of the weight matrix through bilinear interpolation to match the lengths of the input and output. The GEN Tower is designed to accommodate varying input lengths for different tasks and to ultimately generate the output sequence. The model applies learnable additive position encoding. For forecasting task, the training objective is MSE loss.

B.3 Finetuning baselines

Full Finetune and Linear Probe Full finetuning involves updating all parameters of the pretrained model. We observe that using a small learning rate is crucial for stability and performance. In contrast, linear probing only updates the output head while keeping the backbone frozen; a larger learning rate is generally more effective in this case.

LoRA and AdaLoRA LoRA [13] introduces trainable rank-decomposition matrices into the attention layers, enabling parameter-efficient finetuning by injecting updates into a low-rank subspace. AdaLoRA [47] extends LoRA by dynamically allocating the rank during training based on parameter importance, improving adaptation under a parameter budget. For Moirai and Moment, we directly adopt the PEFT library [22] for both LoRA and AdaLoRA. We apply LoRA and AdaLoRA to the query, key, and value projection layers. In addition to the LoRA modules, we also allow the output prediction head to be trainable. The LoRA configuration follows standard settings with rank $r = 16$ and scaling factor $\alpha = 32$. For AdaLoRA, we use the default configuration provided by the PEFT library. Since the original attention implementation in the UNITS codebase uses a large shared weight for query, key, and value, applying LoRA or AdaLoRA from PEFT is not feasible. Therefore, we implement a custom LoRA for it and do not conduct AdaLoRA experiments on UNITS.

Prompt Finetuning For Moirai and Moment, we implement prompt fine-tuning by introducing trainable soft prompt embeddings, which are prepended to the input tokens in the embedding space. We avoid inserting them into the patch token space, as doing so can interfere with the statistical computation of RevIN [14] and offers less expressive capacity compared to the high-dimensional embedding space. During inference, we discard the prompt embeddings from the encoder output and use only the time series embeddings as final representation for prediction. Similarly, only the output head and the prompt embeddings are finetuned, while all other parameters remain frozen. Prompt length is set to 2 by default. For UNITS, we directly use its original prompt tuning implementation.

B.4 Metric details

For long sequence forecasting, we follow the standard protocols to use mean square error (MSE) and mean absolute error for evaluation. For probabilistic forecasting, we include Continuous Ranked Probability Scoremean (CRPS), Mean Scaled Interval Score (MSIS), absolute percentage error (MAPE), symmetric mean absolute percentage error (sMAPE), mean absolute scaled error (MASE), normalized deviation (ND), and normalized root mean squared error (NRMSE) as metrics. The definitions and calculations of probabilistic forecasting metrics are as follows. Note that the notations used here are independent of those in the main text.

Continuous Ranked Probability Score Given a predicted distribution with c.d.f. F and ground truth \mathbf{Y} , the CRPS is defined as:

$$\text{CRPS} = \int_0^1 2\Lambda_\alpha(F^{-1}(\alpha), \mathbf{Y})d\alpha$$

$$\Lambda_\alpha(q, \mathbf{Y}) = (\alpha - \mathbf{1}_{\mathbf{Y} < q})(\mathbf{Y} - q),$$

where Λ_α is the α -quantile loss, also known as the pinball loss at quantile level α .

In practice, the CRPS is intractable or computationally expensive to compute, and we also want to compute a normalized metric, thus we compute a normalized discrete approximation, the mean weighted sum quantile loss, defined as the average of K quantiles:

$$\begin{aligned}\text{CRPS} &\approx \frac{1}{K} \sum_{k=1}^K \text{wQL}[\alpha_k] \\ \text{wQL}[\alpha] &= 2 \frac{\sum_i \Lambda_\alpha(\hat{q}_i(\alpha), \mathbf{Y}_i)}{\sum_i |\mathbf{Y}_i|},\end{aligned}$$

where \mathbf{Y}_i is the ground truth at time step i and $\hat{q}_i(\alpha)$ is the predicted α -quantile at time step i . We take $K = 9$, $\alpha_1 = 0.1$, $\alpha_2 = 0.2, \dots, \alpha_9 = 0.9$ in practice.

Mean Scaled Interval Score The MSIS is a metric to evaluate uncertainty around point forecasts. Given an upper bound prediction, U_i , and lower bound prediction L_i , the MSIS is defined as:

$$\begin{aligned}\text{MSIS} &= \frac{1}{H \cdot \left(\frac{1}{n-m} \sum_{i=m+1}^n |\mathbf{Y}_i - \mathbf{Y}_{i-m}| \right)} \cdot \left[\sum_{i=1}^H (U_i - L_i) \right. \\ &\quad \left. + \frac{2}{a} (L_i - \mathbf{Y}_i) \mathbb{1}_{\{\mathbf{Y}_i < L_i\}} + \frac{2}{a} (\mathbf{Y}_i - U_i) \mathbb{1}_{\{\mathbf{Y}_i > U_i\}} \right]\end{aligned}$$

where $a = 0.05$ is the significance level for a 95% prediction interval, over a forecast horizon of length H , and m is the seasonal factor.

symmetric Mean Absolute Percentage Error The sMAPE is a accuracy measure based on percentage errors, treating over- and under-predictions symmetrically, commonly used in forecasting.

$$\text{sMAPE} = \frac{200}{H} \sum_{i=1}^H \frac{|\mathbf{Y}_i - \hat{\mathbf{Y}}_i|}{|\mathbf{Y}_i| + |\hat{\mathbf{Y}}_i|},$$

Mean Absolute Scaled Error The MASE is a metric for forecasting accuracy, scaling errors by the in-sample mean absolute error of a naive forecast, ensuring interpretability and comparability.

$$\text{MASE} = \frac{1}{H} \sum_{i=1}^H \frac{|\mathbf{Y}_i - \hat{\mathbf{Y}}_i|}{\frac{1}{H-s} \sum_{j=s+1}^H |\mathbf{Y}_j - \mathbf{Y}_{j-s}|},$$

where s is the periodicity of the data. $\mathbf{Y}, \hat{\mathbf{Y}} \in \mathbb{R}^{H \times D}$ are the ground truth and prediction results of the future with H time pints and D dimensions. \mathbf{Y}_i means the i -th future time point.

Normalized Deviation The ND measures prediction accuracy by standardizing deviations between predicted and actual values, aiding model evaluation and optimization.

$$\text{ND} = \frac{1}{H} \sum_{i=1}^H \left| \frac{\mathbf{Y}_i - \hat{\mathbf{Y}}_i}{\mathbf{Y}_i} \right| \times 100\%,$$

Normalized Root Mean Squared Error The NRMSE quantifies prediction error, enables model comparison, aids optimization, and provides interpretable results in time series forecasting.

$$\text{NRMSE} = \frac{\sqrt{\frac{1}{H} \sum_{i=1}^H (\mathbf{Y}_i - \hat{\mathbf{Y}}_i)^2}}{\max(\mathbf{Y}) - \min(\mathbf{Y})}.$$

B.5 Experiment Details

Dataset Construction Unlike pretraining in Moirai, where samples are randomly cropped from time series of varying lengths, we create the training, validation, and test datasets by cropping time series windows with fixed sequence lengths. Given the context and prediction lengths, samples are segmented using a sliding window, where the window size is $C + H$. The train-val-test split follows the default LSF setup. Data are normalized for LSF but not for PF.

Training Setup Since there is no official fine-tuning implementation for Moirai, we configure the training setup as follows. We use the AdamW optimizer with weight decay=0.1, $\beta_1 = 0.9$, and $\beta_2 = 0.98$ for optimization. Specifically, unlike pretraining, which uses a learning rate of $1e-3$, we find that finetuning requires a much smaller learning rate. Based on validation performance, we select a learning rate of either $5e-6$ or $5e-7$ for finetuning our models. The batch size is set to 512 by default for experiments using $\text{MOIRAI}_{\text{Small}}$, and reduced to 256 on $\text{MOIRAI}_{\text{Base}}$ if GPU memory reaches its limit. We adopt a constant learning rate scheduling, and early stopping is employed to monitor training. The context lengths are used directly from the values in the original Moirai models, which are tuned from a range of [1000, 2000, 3000, 4000, 5000]. The patch sizes are also taken from their provided values, which are selected based on data frequency. Since all samples have the same sequence length, sequence packing is not used during training. For Moment and UNITS, we directly follow their provided their original finetuning configurations for experiments, with the learning rate selected from $5e-5$, $5e-6$, or $5e-7$.

Evaluation Setup For Moirai, the evaluation is based on the GluonTS Library [1]. Predictions are sampled 100 times from the learned predictive distributions, and evaluation metrics are computed over those samples. For Moment and UNITS, the LSF metrics are directly computed based on the output predicted series.

Computational environment Our experiments are conducted on a server equipped with an AMD EPYC 7763 CPU (64 cores, 128 threads) and four NVIDIA A40 GPUs, each with 40 GB of memory.

C More Experimental Results

C.1 Further Model Analysis

Effect of Down-Sampling Methods While average pooling is the most commonly used method for generating down-sampled scales, we also investigate two alternative down-sampling techniques to assess their impact. Specifically, we consider *max pooling*, which selects the maximum value within each down-sample kernel, and the *first-step* method, which directly selects the first time step of each kernel. We replace the original average pooling operation in MSFT with these alternatives and evaluate their performance using $\text{MOIRAI}_{\text{Small}}$ on the ETTm1 and ETTm2 datasets. As shown in Figure 6a, the results demonstrate that average pooling consistently outperforms the other two approaches, serving as the most effective method for multi-scale generation.

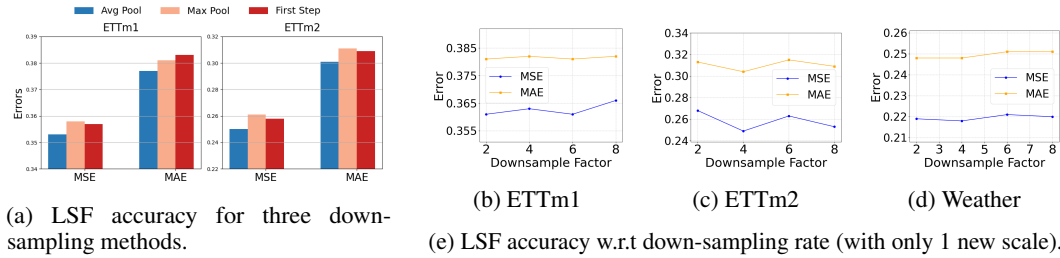


Figure 6: Overview of LSF accuracy comparison.

Effect of Down-Sampling Rate We investigate the effect of down-sampling rate by using only one new scale ($K = 1$) and comparing the results across different down-sampling factors (2, 4, 6, 8). As shown in Figure 6e, the results reveal that the impact of down-sampling rate varies significantly across datasets. For ETTm1 and Weather, the choice of down-sampling factor is relatively less important, with no single down-sample factor is significantly better than the others. In contrast, ETTm2 exhibits a clear pattern: down-sampling factors of 4 and 8 obviously yield better performance, indicating that the periodic patterns in ETTm2 are better captured with these specific factors. These results demonstrate that the effect of down-sampling is dataset-dependent. Furthermore, they indicate that the performance improvement from using multiple scales is not merely due to adding one particularly important scale but rather results from aggregating information across multiple scales.

Attention with Aligned Time Indices In this section, we provide a detailed discussion of the attention misalignment problem and explore another potential solution. As illustrated in Figure 1 (b) and Figure 5 (a), the problem of directly applying self-attention over the concatenated multi-scale sequence is that cross-scale dependencies are biased to the tokens with the same time ID. However, as tokens in different scales represent various resolution, their time indices do not represent the same temporal location information. The tokens in different scales with the same time id do not correspond to the same temporal range (See 1 (b), left part). Therefore, this time ID-induced bias causes attention to learn misleading temporal correlations.

To address this problem, we test another method based on time id alignment during attention operation. As illustrated in Figure 7, when performing attention between two scales, we map the time ID of tokens in the finer scale to the other coarser scale before RoPE, ensuring that finer-scale tokens from the same temporal range share the same time ID as the corresponding coarse-scale token. Consequently, the resulting attention heatmap in Figure 5 (b) eliminates the cross-scale bias caused by time ID, leading to more reasonable temporal correlations between cross-scale tokens.

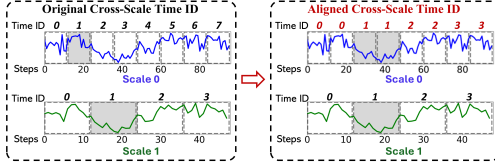


Figure 7: Map the token indices of finer scale to the coarser scale during cross-scale attention

	ETTM1		ETTM2		Weather	
	MSE	MAE	MSE	MAE	MSE	MAE
Naive	0.359	0.380	0.253	0.303	0.219	0.252
Aligned	0.356	0.378	0.250	0.302	0.222	0.254
Ours	0.353	0.377	0.250	0.301	0.216	0.248

Table 7: LSF results for MOIRAI_{Small} using three different attention strategies in MSFT

Table 7 presents the results of the three methods corresponding to the attention patterns in Figure 5. Compared to the Naive method, the time ID alignment approach improves performance on ETTm1 and ETTm2 but shows a performance decline on the Weather dataset. In contrast, our decoupled strategy consistently outperforms both methods. Apart from its inconsistent performance, another limitation of this time ID alignment method is that it is only applicable to Moirai, which employs RoPE for time ID encoding. RoPE allows direct modification of token time IDs during attention, making this adjustment feasible. In contrast, for models using additive position encoding—where positional information is directly added to each token’s input embedding—it is impossible to alter the time ID within the attention blocks. Our method, however, does not rely on modifying time IDs during attention. Instead, it achieves cross-scale alignment through aggregators, making it universally applicable to any model architecture.

Computation Efficiency We compare the memory footprint and training speed of our methods with the following models: PatchTST [25], iTransformer[19], TimesNet [43], and Scaleformer[34]. For Scaleformer, we follow their original implementation and test it on two backbones Autoformer[44] and Informer[49], referred to as Scaleformer-A and Scaleformer-I, respectively. For MSFT, we test its performance on MOIRAI_{Small} and MOIRAI_{Base}, referred to as MSFT-S and MSFT-B. To ensure a fair comparison, we use a consistent batch size of 32 and a context length of 512 across all models, with a prediction length set to 96. To eliminate external interference, the experiments in this section are exclusively conducted on another server equipped with a 12 vCPU Intel(R) Xeon(R) Platinum 8352V CPU @ 2.10GHz and a single RTX 3080 GPU with 20GB of memory.

The results on ETTm1 and Weather datasets are shown in Table 8. The comparison shows that fine-tuning with MSFT on Moirai does not demand more computational resources than other models. Its GPU memory usage is lower than that of alternative methods. In terms of training speed, MSFT achieves a moderate level among the compared methods. However, it significantly outperform Scaleformer, which is also a multi-scale modeling approach.

Table 8: Quantitative comparison of computation efficiency across different methods.

Metric	Dataset	PatchTST	TimesNet	iTransformer	Scaleformer-A	Scaleformer-I	MSFT-S	MSFT-B
Training Speed (ms/iter)	ETTM1	65.92	334.67	27.97	307.36	180.09	103.53	185.38
	Weather	127.67	103.20	28.90	315.44	184.05	110.80	163.93
GPU Memory (MB)	ETTM1	4198	2786	1952	11130	5104	808	1916
	Weather	6866	2592	2110	11138	5106	808	1702

C.2 Full results

We report the full LSF results on four different prediction lengths, with MSE are shown in Table 9 and MAE are shown in Table 10. Results of deep learning-based baselines are obtained from Liu et al. [19] and Chen et al. [4].

Table 9: Full MSE results of long sequence forecasting experiments.

Method	ETTh1				ETTh2				ETTh1				ETTh2				Electricity				Weather				
	96	192	336	720	96	192	336	720	96	192	336	720	96	192	336	720	96	192	336	720	96	192	336	720	
DLinear[2023]	0.345	0.380	0.413	0.474	0.193	0.284	0.369	0.554	0.386	0.437	0.481	0.519	0.333	0.477	0.594	0.831	0.197	0.196	0.209	0.245	0.196	0.237	0.283	0.345	
PatchTST[2023]	0.329	0.367	0.399	0.454	0.175	0.241	0.305	0.402	0.414	0.460	0.501	0.500	0.302	0.388	0.426	0.431	0.195	0.199	0.215	0.256	0.177	0.225	0.278	0.354	
iTransformer[2024a]	0.334	0.377	0.426	0.491	0.180	0.250	0.311	0.412	0.386	0.441	0.487	0.503	0.297	0.380	0.428	0.427	0.148	0.162	0.178	0.225	0.174	0.221	0.278	0.358	
TimeMixer[2024]	0.320	0.361	0.390	0.454	0.175	0.237	0.298	0.391	0.375	0.429	0.484	0.498	0.289	0.372	0.386	0.412	0.153	0.166	0.185	0.225	0.163	0.208	0.251	0.339	
SimpleTM [2025]	0.321	0.360	0.390	0.454	0.173	0.238	0.296	0.393	0.366	0.422	0.440	0.463	0.281	0.355	0.365	0.413	0.141	0.151	0.173	0.201	0.162	0.208	0.263	0.340	
MOIRAI _{Small}	0.404	0.435	0.462	0.490	0.205	0.261	0.319	0.415	0.387	0.418	0.431	0.427	0.287	0.350	0.378	0.403	0.205	0.220	0.236	0.270	0.183	0.229	0.288	0.371	
+ Full finetuning	0.303	0.352	0.388	0.425	0.179	0.234	0.291	0.388	0.382	0.419	0.434	0.426	0.286	0.349	0.376	0.396	0.154	0.172	0.203	0.242	0.154	0.200	0.246	0.311	
+ Linear probing	0.341	0.371	0.402	0.439	0.198	0.258	0.317	0.408	0.384	0.417	0.428	0.425	0.286	0.349	0.377	0.402	0.185	0.200	0.214	0.247	0.167	0.211	0.256	0.315	
+ Prompt tuning	0.335	0.368	0.405	0.428	0.197	0.252	0.304	0.413	0.384	0.415	0.429	0.427	0.286	0.349	0.378	0.403	0.191	0.205	0.219	0.252	0.163	0.207	0.254	0.315	
+ LoRA	0.302	0.357	0.389	0.431	0.179	0.234	0.288	0.387	0.382	0.418	0.431	0.426	0.286	0.349	0.377	0.402	0.152	0.176	0.197	0.243	0.153	0.197	0.243	0.305	
+ AdaLoRA	0.301	0.374	0.406	0.441	0.180	0.234	0.291	0.388	0.381	0.416	0.430	0.427	0.286	0.350	0.378	0.402	0.151	0.175	0.196	0.242	0.154	0.198	0.245	0.305	
+ MSFT	0.295	0.338	0.371	0.409	0.165	0.218	0.267	0.349	0.380	0.416	0.428	0.423	0.279	0.347	0.376	0.392	0.150	0.172	0.193	0.234	0.147	0.189	0.234	0.292	
MOIRAI _{Base}	0.335	0.366	0.391	0.434	0.197	0.250	0.301	0.375	0.375	0.406	0.426	0.440	0.284	0.350	0.378	0.412	0.158	0.174	0.191	0.229	0.163	0.207	0.264	0.350	
+ Full finetuning	0.312	0.355	0.380	0.426	0.176	0.230	0.282	0.344	0.372	0.404	0.423	0.434	0.283	0.355	0.387	0.403	0.144	0.166	0.176	0.207	0.152	0.198	0.250	0.326	
+ Linear probing	0.332	0.369	0.398	0.451	0.188	0.244	0.299	0.375	0.374	0.405	0.424	0.432	0.283	0.355	0.389	0.406	0.155	0.169	0.184	0.221	0.157	0.198	0.245	0.314	
+ Prompt tuning	0.330	0.363	0.389	0.431	0.197	0.247	0.300	0.374	0.375	0.406	0.425	0.440	0.284	0.354	0.392	0.411	0.155	0.168	0.185	0.226	0.159	0.199	0.248	0.314	
+ LoRA	0.311	0.345	0.373	0.414	0.177	0.230	0.280	0.347	0.373	0.404	0.423	0.434	0.284	0.351	0.379	0.411	0.142	0.160	0.178	0.210	0.151	0.198	0.249	0.322	
+ AdaLoRA	0.310	0.346	0.371	0.410	0.175	0.229	0.278	0.351	0.375	0.406	0.424	0.434	0.282	0.352	0.386	0.403	0.142	0.163	0.178	0.207	0.151	0.198	0.253	0.340	
+ MSFT	0.284	0.317	0.343	0.382	0.166	0.217	0.265	0.339	0.372	0.404	0.422	0.429	0.280	0.350	0.379	0.400	0.139	0.159	0.176	0.203	0.144	0.184	0.229	0.296	
MOMENT	-	-	-	-	-	-	-	-	-	-	-	-	-	-	-	-	-	-	-	-	-	-	-	-	
+ Full finetuning	0.297	0.335	0.362	0.412	0.173	0.227	0.277	0.361	0.383	0.413	0.429	0.475	0.288	0.344	0.359	0.397	0.170	0.193	0.227	0.304	0.243	0.299	0.359	0.441	
+ Linear probing	0.304	0.336	0.363	0.417	0.177	0.229	0.277	0.359	0.385	0.418	0.429	0.482	0.290	0.344	0.358	0.397	0.172	0.195	0.229	0.306	0.247	0.303	0.361	0.442	
+ Prompt tuning	0.302	0.339	0.366	0.415	0.176	0.229	0.279	0.359	0.386	0.416	0.429	0.478	0.289	0.345	0.361	0.398	0.172	0.194	0.228	0.304	0.244	0.299	0.360	0.441	
+ LoRA	0.302	0.338	0.366	0.416	0.174	0.226	0.278	0.360	0.384	0.414	0.429	0.473	0.288	0.345	0.359	0.396	0.170	0.193	0.228	0.303	0.242	0.299	0.358	0.440	
+ AdaLoRA	0.302	0.338	0.365	0.416	0.173	0.226	0.276	0.360	0.385	0.414	0.425	0.478	0.288	0.343	0.360	0.396	0.171	0.195	0.230	0.306	0.244	0.301	0.359	0.441	
+ MSFT	0.287	0.327	0.354	0.404	0.170	0.222	0.273	0.356	0.381	0.410	0.426	0.469	0.286	0.341	0.358	0.394	0.166	0.190	0.226	0.300	0.237	0.297	0.356	0.438	
UNITS	0.663	0.694	0.725	0.771	0.226	0.282	0.338	0.436	0.454	0.512	0.548	0.595	0.327	0.410	0.438	0.447	0.367	0.402	0.400	0.559	0.207	0.259	0.311	0.387	
+ Full finetuning	0.338	0.371	0.397	0.472	0.182	0.255	0.316	0.433	0.396	0.428	0.473	0.473	0.469	0.302	0.377	0.421	0.442	0.162	0.178	0.290	0.228	0.172	0.221	0.282	0.352
+ Linear probing	0.342	0.376	0.399	0.477	0.192	0.259	0.317	0.434	0.399	0.439	0.471	0.469	0.306	0.381	0.434	0.445	0.171	0.184	0.202	0.242	0.190	0.247	0.297	0.363	
+ Prompt tuning	0.359	0.399	0.439	0.526	0.184	0.259	0.326	0.444	0.382	0.428	0.467	0.474	0.306	0.378	0.424	0.436	0.159	0.179	0.193	0.231	0.159	0.212	0.269	0.346	
+ LoRA	0.338	0.370	0.396	0.466	0.183	0.256	0.315	0.431	0.377	0.426	0.463	0.481	0.300	0.379	0.422	0.433	0.163	0.170	0.192	0.228	0.163	0.214	0.274	0.349	
+ MSFT	0.336	0.366	0.396	0.461	0.179	0.248	0.313	0.405	0.376	0.428	0.463	0.469	0.302	0.375	0.416	0.425	0.154	0.169	0.186	0.227	0.158	0.204	0.261	0.342	

Table 10: Full MAE results of long sequence forecasting experiments.

Method	ETTm1				ETTm2				ETTh1				ETTh2				Electricity				Weather			
	96	192	336	720	96	192	336	720	96	192	336	720	96	192	336	720	96	192	336	720	96	192	336	720
DLinear[2023]	0.372	0.389	0.413	0.453	0.292	0.362	0.427	0.522	0.400	0.432	0.459	0.516	0.387	0.476	0.541	0.657	0.282	0.285	0.301	0.333	0.255	0.296	0.335	0.381
PatchTST[2023]	0.367	0.385	0.410	0.439	0.259	0.302	0.343	0.400	0.419	0.445	0.466	0.488	0.348	0.400	0.433	0.446	0.285	0.289	0.305	0.337	0.218	0.260	0.297	0.348
iTransformer[2024a]	0.368	0.391	0.420	0.459	0.264	0.309	0.348	0.407	0.405	0.436	0.458	0.491	0.349	0.400	0.432	0.445	0.240	0.253	0.269	0.317	0.214	0.254	0.296	0.349
TimeMixer[2024]	0.357	0.381	0.404	0.441	0.258	0.299	0.340	0.396	0.400	0.421	0.458	0.482	0.341	0.392	0.414	0.434	0.247	0.256	0.277	0.310	0.209	0.250	0.287	0.341
SimpleTM [2025]	0.361	0.380	0.404	0.438	0.257	0.299	0.338	0.395	0.392	0.421	0.438	0.462	0.338	0.387	0.401	0.436	0.235	0.247	0.267	0.293	0.207	0.248	0.290	0.341
MOIRAI _{Small}	0.383	0.402	0.416	0.437	0.282	0.338	0.355	0.410	0.402	0.423	0.435	0.450	0.334	0.374	0.395	0.421	0.299	0.310	0.323	0.347	0.216	0.258	0.297	0.346
+ Full finetuning	0.345	0.372	0.393	0.419	0.251	0.292	0.329	0.390	0.400	0.423	0.438	0.453	0.332	0.372	0.392	0.416	0.242	0.265	0.289	0.319	0.189	0.236	0.272	0.317
+ Linear probing	0.360	0.382	0.401	0.425	0.274	0.315	0.352	0.406	0.399	0.423	0.436	0.451	0.333	0.373	0.394	0.420	0.278	0.289	0.302	0.328	0.201	0.243	0.277	0.317
+ Prompt tuning	0.359	0.380	0.403	0.423	0.273	0.309	0.343	0.409	0.402	0.423	0.435	0.451	0.337	0.373	0.394	0.420	0.285	0.294	0.307	0.331	0.199	0.241	0.276	0.317
+ LoRA	0.344	0.374	0.394	0.421	0.250	0.290	0.327	0.390	0.399	0.423	0.435	0.450	0.333	0.373	0.394	0.420	0.244	0.266	0.285	0.321	0.189	0.233	0.271	0.315
+ AdaLoRA	0.342	0.381	0.399	0.423	0.255	0.294	0.332	0.393	0.399	0.422	0.435	0.450	0.334	0.373	0.394	0.420	0.244	0.265	0.285	0.321	0.189	0.233	0.271	0.315
+ MSFT	0.341	0.367	0.387	0.414	0.242	0.281	0.314	0.368	0.401	0.421	0.433	0.449	0.326	0.369	0.391	0.413	0.241	0.262	0.282	0.316	0.185	0.229	0.266	0.311
MOIRAI _{Base}	0.360	0.379	0.394	0.419	0.271	0.306	0.339	0.388	0.398	0.417	0.429	0.452	0.334	0.380	0.405	0.432	0.248	0.263	0.278	0.307	0.198	0.240	0.282	0.338
+ Full finetuning	0.334	0.361	0.380	0.409	0.248	0.283	0.315	0.367	0.396	0.416	0.428	0.451	0.330	0.378	0.402	0.427	0.236	0.256	0.267	0.295	0.186	0.235	0.278	0.333
+ Linear probing	0.350	0.372	0.393	0.419	0.269	0.304	0.335	0.379	0.396	0.416	0.428	0.451	0.333	0.378	0.402	0.427	0.240	0.260	0.271	0.298	0.189	0.236	0.278	0.333
+ Prompt tuning	0.355	0.377	0.393	0.417	0.271	0.301	0.339	0.387	0.397	0.416	0.428	0.452	0.335	0.378	0.404	0.432	0.246	0.268	0.274	0.305	0.196	0.235	0.272	0.313
+ LoRA	0.337	0.359	0.379	0.407	0.248	0.289	0.327	0.366	0.397	0.416	0.429	0.451	0.334	0.378	0.405	0.431	0.234	0.252	0.269	0.296	0.186	0.235	0.278	0.342
+ AdaLoRA	0.336	0.361	0.379	0.407	0.251	0.286	0.321	0.368	0.397	0.416	0.429	0.450	0.331	0.376	0.401	0.427	0.235	0.256	0.267	0.296	0.186	0.235	0.278	0.342
+ MSFT	0.335	0.359	0.378	0.404	0.246	0.285	0.320	0.369	0.395	0.415	0.429	0.450	0.327	0.374	0.404	0.427	0.230	0.252	0.266	0.293	0.182	0.234	0.261	0.311
MOMENT																								
+ Full finetuning	0.348	0.369	0.386	0.415	0.262	0.299	0.332	0.386	0.406	0.424	0.445	0.485	0.348	0.386	0.404	0.437	0.276	0.292	0.313	0.363	0.240	0.287	0.328	0.384
+ Linear probing	0.353	0.370	0.385	0.414	0.265	0.300	0.333	0.385	0.406	0.429	0.445	0.490	0.350	0.387	0.404	0.437	0.278	0.294	0.314	0.364	0.246	0.290	0.330	0.384
+ Prompt tuning	0.350	0.371	0.387	0.416	0.264	0.299	0.332	0.385	0.406	0.426	0.443	0.486	0.349	0.388	0.406	0.438	0.278	0.293	0.314	0.362	0.243	0.284	0.330	0.384
+ LoRA	0.351	0.370	0.387	0.416	0.262	0.298	0.333	0.385	0.407	0.425	0.439	0.484	0.349	0.387	0.404	0.438	0.278	0.292	0.314	0.361	0.239	0.285	0.328	0.384
+ AdaLoRA	0.351	0.370	0.387	0.415	0.262	0.298	0.331	0.384	0.407	0.426	0.438	0.487	0.349	0.386	0.405	0.437	0.277	0.292	0.314	0.364	0.242	0.288	0.329	0.385
+ MSFT	0.345	0.366	0.383	0.412	0.259	0.295	0.328	0.381	0.404	0.422	0.436	0.481	0.347	0.384	0.403	0.435	0.274	0.290	0.311	0.360	0.233	0.284	0.328	0.383
UNITS																								
+ Full finetuning	0.520	0.541	0.561	0.588	0.301	0.333	0.367	0.420	0.444	0.478	0.495	0.547	0.362	0.412	0.441	0.455	0.438	0.467	0.465	0.482	0.254	0.294	0.328	0.376
+ Linear probing	0.513	0.530	0.549	0.575	0.297	0.328	0.361	0.415	0.439	0.472	0.489	0.541	0.356	0.402	0.431	0.445	0.429	0.458	0.457	0.473	0.253	0.293	0.327	0.375
+ Prompt tuning	0.513	0.533	0.551	0.575	0.295	0.326	0.359	0.419	0.443	0.475	0.492	0.543	0.356	0.402	0.431	0.445	0.429	0.458	0.457	0.473	0.253	0.293	0.327	0.375
+ LoRA	0.391	0.411	0.436	0.482	0.270	0.318	0.359	0.431	0.399	0.427	0.447	0.460	0.347	0.395	0.430	0.446	0.259	0.277	0.290	0.321	0.206	0.254	0.295	0.347
+ MSFT	0.372	0.390	0.408	0.451	0.265	0.315	0.352	0.418	0.397	0.427	0.446	0.466	0.352	0.398	0.431	0.447	0.259	0.266	0.285	0.316	0.211	0.256	0.299	0.348
+ MSFT	0.372	0.388	0.408	0.445	0.267	0.311	0.349	0.403	0.392	0.421	0.446	0.461	0.353	0.395	0.427	0.444	0.252	0.266	0.282	0.315	0.208	0.249	0.290	0.342

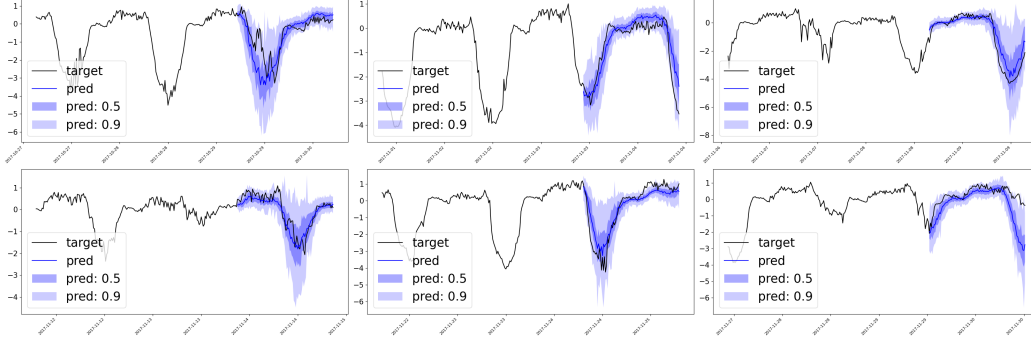


Figure 8: Visualization on ETTm1 (predict-96)

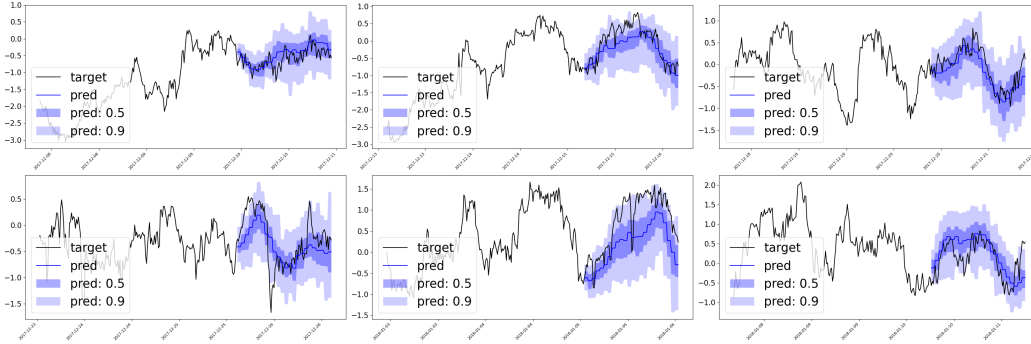


Figure 9: Visualization on ETTm2 (predict-96)

C.3 Forecast Visualizations

We visualize the forecasting predictions of MSFT using $\text{MOIRAI}_{\text{Small}}$ on ETTm1 and ETTm2, with the models finetuned on the predict-96 setup. In addition to the point forecast, which is the median of the samples, the 0.5 and 0.9 quantiles are also plotted for illustration. Only part of the context series is included in the plots.

D Limitation and Future Work

As indicated in our experiments, MSFT consistently delivers outstanding finetuning results on encoder-based TSFMs, validating the effectiveness of incorporation of multi-scale modeling into TSFM finetuning. However, a natural question that one may be curious about is how to apply our multi-scale finetuning method to TSFMs with other structures, such as decoder-based models.

Here, we first clarify why we focus solely on encoder-based TSFMs in this paper. First, encoder-based models are more flexible to prediction length, making them more efficient to finetune on standard LSF datasets. In contrast, decoder-based models, due to their auto-regressive nature, are significantly slower when finetuning and predicting on long time series. Although some decoder-based models provide finetuning examples, they are often applied to limited datasets without following the standard LSF pipeline. For example, TimesFM are only finetuned on a subset of ETTm dataset for the predict-96 setup. This limitation hinders comprehensive comparisons between our methods and existing LSF baselines or other fine-tuning approaches. Secondly, decoder-based models inherently employ causal masking in their attention mechanisms, which imposes a specific dependency structure. As a pioneering study, we choose to use encoder-based models without such constraints, providing greater flexibility and generality.

Despite the aforementioned challenges, we provide a potential direction for applying MSFT to decoder-based models. Due to their auto-regressive nature, the causal attention mechanism in decoder-only models can only attend to preceding tokens in the sequence, rather than all tokens

simultaneously. Therefore, the creation of multi-scale embedding sequence needs to take the order of scales into account. Similar to Scalerformer[34], we arrange the scales in a coarse-to-fine order and sequentially using coarse information to refine the fine-grained predictions at subsequent levels. First, we concatenate the multi-scale input embeddings as $\mathbf{h}_0 = \text{Concat}(\mathbf{h}_K^0, \mathbf{h}_{K-1}^0, \dots, \mathbf{h}_0^0)$, ensuring the scales are in a coarse-to-fine order. Then, for the attention, we keep using the in-scale masking on the original causal masking, ensuring that the tokens can only attend to the previous tokens from the same scale. Regarding cross-scale aggregators, the original dual-branch design cannot be directly applied due to the auto-regressive nature. Instead, we adopt a single coarse-to-fine branch to fuse the token-level information. The multi-scale mixing remains unchanged, enabling the aggregation of predictions across different scales. We leave the further exploration of this direction as a future work.

Another potential limitation is that multi-scale modeling increases the number of input tokens due to the introduction of new scales. Given the transformer’s $\mathcal{O}(N^2)$ complexity with respect to input sequence length, this inevitably increases the computational cost. On the other hand, finetuning with new scales can exceed the upper bound of fine-tuning performance achieved on a single scale. Consequently, a trade-off exists between computational cost and performance. Another future direction is to further investigate this trade-off and develop a more efficient strategy to achieve an optimal balance.